Roy *et al.*
*Protection and Control of Modern Power Systems* (2023) 8:8
https://doi.org/10.1186/s41601-023-00281-2

Protection and Control of Modern Power Systems

ORIGINAL RESEARCH

Open Access

# Robust backstepping global integral terminal sliding mode controller to enhance dynamic stability of hybrid AC/DC microgrids

Tushar Kanti Roy[1*], Subarto Kumar Ghosh[2] and Sajeeb Saha[3]

**Abstract**

In this paper, a Backstepping Global Integral Terminal Sliding Mode Controller (BGITSMC) with the view to enhancing the dynamic stability of a hybrid AC/DC microgrid has been presented. The proposed approach controls the switching signals of the inverter, interlinking the DC-bus with the AC-bus in an AC/DC microgrid for a seamless interface and regulation of the output power of renewable energy sources (Solar Photovoltaic unit, PMSG-based wind farm), and Battery Energy Storage System. The proposed control approach guarantees the dynamic stability of a hybrid AC/DC microgrid by regulating the associated states of the microgrid system to their intended values. The dynamic stability of the microgrid system with the proposed control law has been proved using the Control Lyapunov Function. A simulation analysis was performed on a test hybrid AC/DC microgrid system to demonstrate the performance of the proposed control strategy in terms of maintaining power balance while the system's operating point changed. Furthermore, the superiority of the proposed approach has been demonstrated by comparing its performance with the existing Sliding Mode Control (SMC) approach for a hybrid AC/DC microgrid.

**Keywords** Dynamic stability, Hybrid AC/DC microgrids, Power balance, Robust backstepping controller, Global integral terminal sliding mode controller, Switching control signals

## 1 Introduction

With ever-increasing electricity demand, dwindling fossil fuel reserves, and the Greenhouse Gas (GHG) impact on electrical power systems, green Renewable Energy Source (RES) has emerged as the preferred alternative to nonrenewable energy sources or fossil fuels [1, 2]. The Distributed Generation (DG) concept has played a significant role in the transition from conventional fossil fuel-based energy sources to cleaner RES over the last two decades [3]. RES, such as Solar Photovoltaic (PV) and wind energy, are abundant around the world, and they are regarded as the key contributors to improving carbon sustainability [4, 5]. And it is commonly adopted alongside an Energy Storage System (ESS) to form a Microgrid (MG) and serve local electricity demand. The primary benefits of an MG includes to increase dependability, autonomous control, and the flexibility to satisfy local load needs in both islanded (without grid support) and grid-connected modes [6, 7].

However, the intermittencies associated with the RES and the fluctuations in load demands are considered the major issues for MG operators [8, 9]. For example, the generation of wind and solar energy systems, which are the most common RES that features in the MG, depends on the weather conditions (solar irradiation and wind speed). In order to mitigate the intermittencies associated with RES and best utilize their benefits, the Battery

*Correspondence:
Tushar Kanti Roy
tkroy@ete.ruet.ac.bdmailto; tkroy@ete.ruet.ac.bd
[1] Department of Electronics & Telecommunication Engineering, Rajshahi University of Engineering and Technology, Rajshahi 6204, Bangladesh
[2] Department of Electrical and Electronic Engineering, Rajshahi University of Engineering and Technology, Rajshahi 6204, Bangladesh
[3] School of Science, Technology and Engineering, University of the Sunshine Coast, Moreton Bay Campus, Queensland, Australia

ESS (BESS) has become an indispensable component in an MG system [9]. Solar energy and BESS primarily deal with DC electricity, which can be directly used to power DC loads [10, 11]. This will simplify the control structure because the frequency and reactive power regulation are not required in DC operation [12, 13, 26]. Similarly, RES that generates AC power can be utilized to power the AC loads, obviating the need for rectifiers to power DC loads [14]. As a result, hybrid AC/DC MGs with RESs are quickly increasing and capturing the attention of many researchers [15, 16]. An AC/DC MG combines the advantages of both the AC and DC MGs [17, 18], which can handle both the AC and DC loads without the requirement for further AC-to-DC and DC-to-AC conversions. Furthermore, for a hybrid AC/DC MG, when both AC and DC MG are connected with a Bidirectional Voltage Source Converter (BVSC) reduces the number of conversion steps while simplifying control operations in the MG [13, 19, 26]. However, dealing with intermittencies in RES and fluctuations in loads, and the energy management of diverse components is regarded as a key challenge for the MG operator. Therefore, robust controllers are essential for hybrid AC/DC MGs to provide resiliency against the aforementioned challenges.

Different linear and nonlinear controllers for controlling individual DC and AC MGs have been designed and implemented in the existing literature [20–23]. The overall aim of these controllers is to maintain the dynamic stability of a MG regardless of whether they are DC or AC. Liu, et al., [23] and Ma et al., [24], identified that a model free Proportional-Integral (PI) controller can be used to manage the output power of each of the components in hybrid AC/DC MGs where power regulation is achieved by coordinating the actions of individual component controllers. However, the PI controller is not capable to ensure the dynamic stability of hybrid AC/DC MGs under severe system transients. Sowmmiya and Govindharajan, [25] proposed a similar controller for a hybrid AC/DC MG to manage the grid voltage and frequency. In contrast, a distributed control system is proposed in [26] to coordinate the Multiple Parallel Bidirectional Power Converter (MPBPC) in a hybrid AC/DC MG. However, the dynamical stability of DC-and AC-bus voltages has not been considered in the control approach in [26], though the regulation of these voltages is essential for the desired power-sharing in the MG.

Loh et al. [27] proposed a generalized droop control strategy that assures the dynamic stability of the DC-bus voltage in a hybrid AC/DC MG while ensuring acceptable power-sharing. However, Loh et al. [27] did not consider the power-sharing between the AC and DC sides of the hybrid MG. Moreover, it is well-known that linear controllers suffer from performance deficiencies while seeking to reduce quick transients, such as an abrupt change in generation, a sudden shift in load, a short-circuit fault, etc. To overcome this drawback, an improved droop control approach has been proposed in [28] to derive the switching signals for the bidirectional VSC, allowing power to be exchanged between the AC and DC-sides of a hybrid MG. The fundamental issue with such droop controllers is their sensitivity to voltage fluctuations at the DC-or AC-buses of the MG where components of the MG are connected. Furthermore, as droop controllers in a hybrid AC/DC MG are developed using linear characteristics of individual MG components, there is a greater risk of such voltage fluctuations. Also, the unpredictability of RES causes the MG to operate over a wide spectrum. Therefore, the linear droop controllers are incapable of maintaining the dynamic stability of a hybrid AC/DC MG due to their wide operating range.

Besides linear controllers, several nonlinear control techniques for enhancing the transient stability of hybrid AC/DC MGs have been proposed in the current literature [29–31]. The nonlinear controllers are expected to provide better performance as compared to linear controllers since these controllers are developed based on the nonlinear dynamical models of a hybrid AC/DC MG, which can describe the system dynamics under a wide range of operating conditions [24]. Adaptive Neural Network (ANN-based controllers have been presented in [32–34], to capture nonlinearities associated with different components of a hybrid AC/DC MG. However, the performance of this ANN based controller is dependent on the adequate amount and accuracy of the training data set. This issue associated with the training data set can be solved by the application of model-based control strategies. A model based nonlinear backstepping controller for a hybrid AC/DC MG has been presented in [1, 35], which considers dynamics associated with each of the components in the MG to ensure acceptable dynamic performance under a wide range of operating conditions. Though the controller in [1, 35] can attain the desired power balance, it is vulnerable to external disturbances (EDs), such as generation or load variations, parameter variations, and faults, which are common during the operation of the MG. To alleviate this limitation, Armghan et al. [29, 31] proposed an adaptive backstepping-based nonlinear control scheme that assures DC-bus voltage regulation. However, the proposed approach is only applicable to the islanded mode operation of the MG.

EDs can be included in the dynamic model as unknown disturbances to capture the modeling errors, parametric uncertainties, and measurement noises associated with a hybrid AC/DC MG. Wang et al., [36] presents a

nonlinear disturbance observer-based control technique for a hybrid AC/DC MG, where the observer is used to estimate the unknown disturbance and to assist the controller in adjusting the DC bus voltage to the desired value under these disturbances. However, the control actions are derived using PI scheme, which is expected to be compromised due to the estimation error of the disturbance observer.

As discussed in [37, 38], the Sliding Mode Controller (SMC) is well known for its resilience against parametric uncertainty and EDs. A nonlinear SMC with droop characteristics has been proposed in [39], where the primary goal was to regulate the grid voltage and current considering only the dynamics associated with the BVSC. The presented control approach does not include the dynamics associated with the RES and BESS, even though they have a major influence on the overall dynamic stability of a hybrid AC/DC MG. Considering these facts, Baghaee et al. [40] demonstrated a nonlinear SMC scheme for all the associated components in a hybrid AC/DC MG. Though the SMC approach can properly accomplish DC-bus voltage regulation, it exhibits an unexpected chattering issue. To address the chattering issue, Armghan et al. [29, 31] explored a double-integral based SMC for a PV and wind-based grid-connected hybrid AC/DC MG without considering any ESS. Furthermore, Armghan et al. [29, 31] did not consider neither parametric nor external uncertainties. To overcome this drawback, Hassan et al., [41] designed an adaptive Lyapunov redesign strategy for power converters connected to RES and hybrid ESS considering uncertainties associated with the system. Though it ensures DC-bus voltage regulation and energy management, it does not consider the dynamics of the associated DC–AC converter.

Based on the presented literature review, it is evident that a hybrid AC/DC MG with different types of RES-based distributed energy sources, ESS, and associated AC/DC loads are difficult to maintain within the desired operating boundary. With a view to addressing this challenge, this paper proposes a Backstepping Global Integral Terminal Sliding Mode Controller (BGITSMC) for a hybrid AC/DC MG with RES and ESS incorporating EDs associated with MGs, which builds on the approach in [36]. The proposed BGITSMC approach assures the overall dynamic stability of the hybrid AC/DC MG by deriving control inputs in such a way that assures all the associated system states of the MG converge to their intended values. EDs have been incorporated into the dynamical models of various components in hybrid AC/DC MGs, and the proposed control is designed considering the effects of these disturbances. Overall dynamic stability of the MG with the proposed controller has been demonstrated using the control Lyapunov function. The superior performance of the proposed control approach has been demonstrated through rigorous simulation studies and compared with that of the existing SMC (ESMC).

## 2 Brief overview of a hybrid AC/DC MG

A schematic diagram of a hybrid AC/DC MG is presented in Fig. 1. As illustrated in the figure, a hybrid AC/DC MG comprises a DC part and an AC part. The DC part includes all the DC components: DC energy source (solar energy source, PMSG-based wind energy sources), BESS, DC loads, and associated power electronic device [DC–DC Boost Converter (DBC)], and forms a DC MG. On the other hand, the AC part includes the AC loads, which are interfaced with the DC side using a BVSC. Due to the influence of weather intermittencies on the generation of the RES and the load variation, a hybrid AC/DC MG exhibits transients if there is any variation in its operating condition. The control actions associated with the controllable entities in the MG are required to be adjusted to deal with such transients and ensure the dynamic stability of the MG. For example, the DBCs associated with the solar PV units in a MG are required to be regulated to manage output power while assuring the extraction of maximum possible power under varying weather conditions. Similarly, the associated PMSG's switching control inputs are regulated to extract the maximum output power from the wind farm, while the DC-DC Bidirectional Converter (DBBC) associated with the BESS is regulated to control its charging and discharging current. Also, the switching signal driving the BVSC interfacing the DC and AC sides of the MG must also be adjusted according to the intended power exchange between the two sides of the MG to maintain its dynamic stability under varying loads and generation as well as EDs. The accuracy and completeness of the model describing the MG, while deriving its controller. Moreover, the dynamic models of each components of a MG are required to be considered to capture the complete dynamics and to

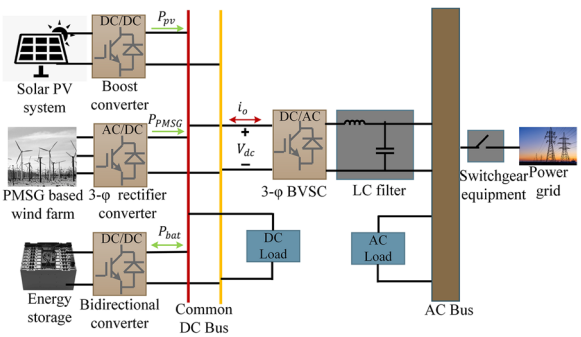


**Fig. 1** Schematic diagram of the proposed hybrid AC/DC MG

ensure the overall stability of the MG. In the following, first dynamic modeling of the individual components of a hybrid AC/DC MG is developed, followed by the derivation of the proposed controller using the developed dynamic model of the MG.

## 3 Dynamical model of a hybrid AC/DC MG

This section presents a dynamic model describing each of the components of a hybrid AC/DC MG, which will be used in the following section to develop the proposed controller for the MG. A dynamic model of the BVSC with an output LC filter, which is used to interface the DC and AC sides of the hybrid MG, is presented first. This is followed by a dynamic model of a solar PV unit with DBC, a PMSG-based wind farm with a DBC, the BESS with a DBBC.

### 3.1 Modeling of the BVSC with an output LC filter

The equivalent circuit of a BVSC with an output LC filter is shown in Fig. 2, and the dynamical model of this converter can be developed using circuit theories which are described as follows [22]: with an LC filter.

$$\begin{aligned}
\frac{dV_{dc}}{dt} &= \frac{i_o}{C_{dc}} - \frac{3}{2V_{dc}C_{dc}}V_{cd}I_{od} \\
\frac{dV_{cd}}{dt} &= \frac{1}{C_f}I_{id} + \omega V_{cq} - \frac{1}{C_f}I_{od} \\
\frac{dV_{cq}}{dt} &= \frac{1}{C_f}I_{iq} - \omega V_{cd} - \frac{1}{C_f}I_{oq} \\
\frac{dI_{id}}{dt} &= -\frac{1}{L_f}V_{cd} + \omega I_{iq} + \frac{1}{L_f}V_{dc}M_d \\
\frac{dI_{iq}}{dt} &= -\frac{1}{L_f}V_{cq} - \omega I_{id} + \frac{1}{L_f}V_{dc}M_q
\end{aligned} \tag{1}$$

where $V_{dc}$ is the DC-link voltage across the capacitor $C_{dc}$, $i_o$ is the current flowing in or out at the DC-bus, $V_{cd}$ is the direct-axis voltage across the filter capacitor ($C_f$), $V_{cq}$ is the quadrature-axis voltage across the filter capacitor, $\omega$ is the angular frequency, $I_{id}$ is the direct-axis current at the input of the $LC$ filter, $I_{iq}$ is the quadrature-axis current at the input of the $LC$ filter,$I_{od}$ is the direct-axis current at the output of the $LC$ filter, $I_{oq}$ is the quadrature-axis current at the output of the $LC$ filter, $L_f$ is the filter inductance, $M_d$ is the direct-axis switching signal of the VSC, and $M_q$ is the quadrature-axis switching signal of the VSC. By incorporating external EDs into Eq. (1), it can be written as:

$$\begin{aligned}
\frac{dV_{dc}}{dt} &= \frac{i_o}{C_{dc}} - \frac{3}{2V_{dc}C_{dc}}V_{cd}I_{od} + d_1 \\
\frac{dV_{cd}}{dt} &= \frac{1}{C_f}I_{id} + \omega V_{cq} - \frac{1}{C_f}I_{od} + d_2 \\
\frac{dV_{cq}}{dt} &= \frac{1}{C_f}I_{iq} - \omega V_{cd} - \frac{1}{C_f}I_{oq} + d_3 \\
\frac{dI_{id}}{dt} &= -\frac{1}{L_f}V_{cd} + \omega I_{iq} + \frac{1}{L_f}V_{dc}M_d + d_4 \\
\frac{dI_{iq}}{dt} &= -\frac{1}{L_f}V_{cq} - \omega I_{id} + \frac{1}{L_f}V_{dc}M_q + d_5
\end{aligned} \tag{2}$$

where $d_1$, $d_3$, $d_3$, $d_4$, and $d_5$ are EDs for the BVSC with an output LC filter and the proposed control approach will be used to obtain the switching control inputs, $S_d$ and $S_q$.

### 3.2 Modeling of the solar PV unit with a DBC

The comparable circuit shown in Fig. 3 will be used to generate a dynamical model of a solar PV unit with a DBC, with the PV cell assumed to be a single diode model. The detailed dynamical model can be represented by the equations shown below [1]:

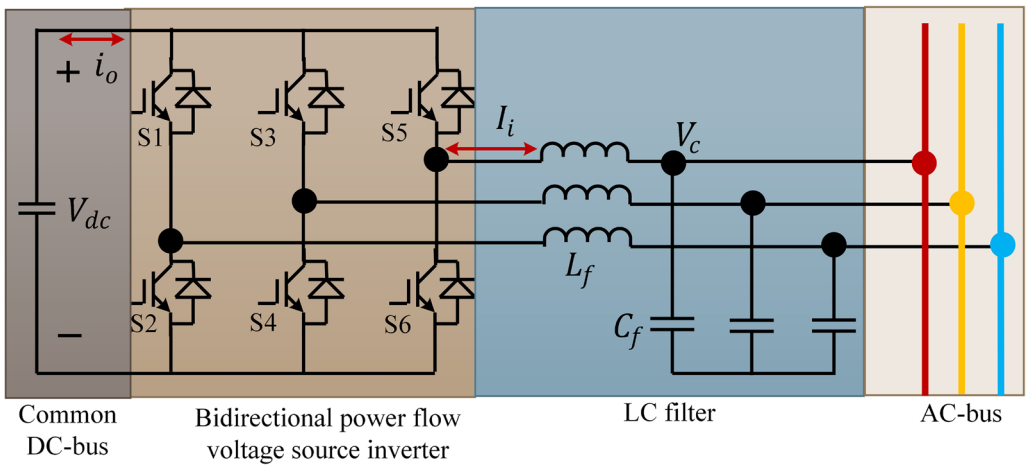


**Fig. 2** An equivalent circuit diagram of the BVSC

$$\begin{aligned}\frac{di_{Lpv}}{dt} &= \frac{1}{L_{Lpv}}\left[-r_{Lpv}i_{Lpv} - \left(1-\mu_{pv}\right)v_{dc} + v_{pv}\right]\\ \frac{dv_{dc}}{dt} &= \frac{1}{C_{dc}}\left[\left(1-\mu_{pv}\right)i_{Lpv} - i_{opv}\right]\end{aligned} \tag{3}$$

where $v_{pv}$, $i_{Lpv}$, $C_{dc}$, $i_{opv}$, and $\mu_{pV}$ are the solar PV unit's output voltage, the current flowing through the internal inductance ($L_{Lpv}$), and resistance ($r_{Lpv}$) of the converter, DC-bus capacitance, load current, and control signal, respectively. With the EDs in the PV unit with the DBC, the dynamical model in Eqs. (3) can be written as follows:

$$\begin{aligned}\frac{di_{Lpv}}{dt} &= \frac{1}{L_{Lpv}}\left[-R_{pv}i_{Lpv} - \left(1-u_{pv}\right)v_{dc} + v_{pv}\right] + d_6\\ \frac{dv_{dc}}{dt} &= \frac{1}{C_{dc}}\left[\left(1-u_{pv}\right)i_{Lpv} - i_{opv}\right] + d_7\end{aligned} \tag{4}$$

where $d_6$, $d_7$ are the EDs for the DBC in the PV system.

### 3.3 Modeling of the PMSG-based wind farm

The rectifier is directly linked to the stator in a PMSG based wind farm, as illustrated in Fig. 4, and the rectifier's output is connected to the DC-bus through a DBC. The DC-bus dynamic, on the other hand, is not considered while building the controller for this PMSG-based wind because it has already been addressed by all other components. The stator current dynamics may be used to illustrate the dynamical model of a PMSG-based wind farm, as shown below [20]:

$$\begin{aligned}\frac{di_{sd}}{dt} &= -\frac{R_s}{L_s}i_{sd} + \omega_s i_{sq} + \frac{1}{L_s}V_{dc}m_{sd}\\ \frac{di_{sq}}{dt} &= -\frac{R_s}{L_s}i_{sq} - \omega_s i_{sd} - \frac{\omega_s\psi}{L_s} + \frac{1}{L_s}V_{dc}m_{sq}\end{aligned} \tag{5}$$

where $i_{sd}$ is a direct-axis component of the stator current, $i_{sq}$ is a quadrature-axis component of the stator current, $R_s$ is the stator resistance, $L_s$ is the stator inductance, $\omega_s$ is the angular frequency of the synchronously rotating frame, $\psi$ is the stator flux, $m_{sd}$ is the direct-axis switching control signal for the rectifier, and $m_{sq}$ is the quadrature-axis switching control signal for the rectifier. The AC power from the PMSG is converted to DC power before being fed into the DC-bus through a rectifier. The rectified current of a diode rectifier can be computed using an average value model, which is expressed as follows:

$$\frac{d_{i_R}}{dt} = \frac{1}{2L_s}\left(\frac{3\sqrt{6}}{\pi}E - v_R - \frac{3}{\pi}L_s\omega_s i_R\right) \tag{6}$$

where $i_R$ is the rectifier current, $E$ is the per phase rms value of the PMSG, and $v_R$ is the output voltage of the rectifier. As previously stated, the rectifier's output is fed to the DC-bus through a DBC. As a result, the DBC dynamic can be written as follows:

$$\begin{aligned}\frac{di_R}{dt} &= \frac{1}{L_R}[-r_R i_R - (1-u_R)v_{dc} + v_R]\\ \frac{dv_{dc}}{dt} &= \frac{1}{C_{dc}}[(1-u_R)i_R - i_{oR}]\end{aligned} \tag{7}$$

where $i_R$, $i_{oR}$, and $u_R$ represent the current flowing through the inductance ($L_R$), and internal resistance ($r_R$) of the converter, load current, and control signal, respectively. When the effects of various environmental conditions are factored into Eqs. (7), the following result is obtained:

$$\begin{aligned}\frac{di_R}{dt} &= \frac{1}{L_R}[-r_R i_R - (1-u_R)v_{dc} + v_R] + d_8\\ \frac{dv_{dc}}{dt} &= \frac{1}{C_{dc}}\left[(1-u_R)i_{L_R} - i_{oR}\right] + d_9\end{aligned} \tag{8}$$

where $d_8$ and $d_9$ are the EDs which are used to capture variations or modeling errors in the relevant equations. Using the proposed robust control technique, this dynamical model is utilized to develop the control input.

### 3.4 Modeling of the BESS with the DBBC

The equivalent circuit of a BESS along with a converter is shown in Fig. 5 and the dynamical model can.

be obtained based on this figure which can be written as:

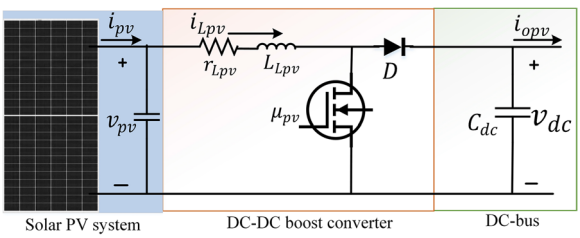


**Fig. 3** The DBC equivalent circuit for the solar PV system

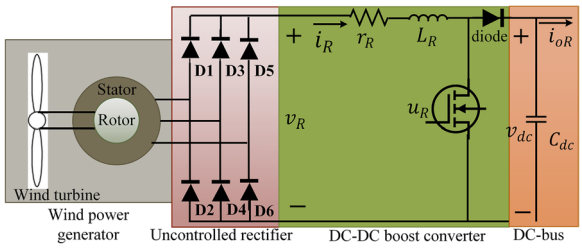


**Fig. 4** The equivalent circuit diagram of the PMSG with an uncontrolled rectifier converter

$$\begin{aligned}\frac{di_{bat}}{dt} &= \frac{1}{L_{bat}}(v_{bat} - r_{bat}i_{bat} - \mu_{bat}v_{dc})\\ \frac{dv_{dc}}{dt} &= \frac{1}{C_{dc}}(\mu_{bat}i_{bat} - i_{obat})\end{aligned} \tag{9}$$

where $i_{bat}, v_{bat}, L_{bat}, r_{bat}, i_{obat}$, and $\mu_{bat}$ are used to represent the output current of the BESS, the terminal voltage of the battery, the inductance of the converter, the internal resistance of the inductance, the load current, and the switching control signal, respectively. The dynamical model of the BESS with a DBBC in Eqs. (9) can be represented by integrating external disturbances:

$$\begin{aligned}\frac{di_{bat}}{dt} &= \frac{1}{L_{bat}}(v_{bat} - r_{bat}i_{bat} - \mu_{bat}v_{dc}) + d_{10}\\ \frac{dv_{dc}}{dt} &= \frac{1}{C_{dc}}(\mu_{bat}i_{bat} - i_{obat}) + d_{11}\end{aligned} \tag{10}$$

where the EDs $d_{10}$ and $d_{11}$ represent the fluctuations or modeling mistakes in the appropriate equations. The switching control input for the DBBC is designed using the dynamical model described by Eq. (10).

In the following section, these dynamic models describing different components of the hybrid MG are used to develop the proposed controller.

## 4 Proposed controller design

The switching signals for all the power electronic converters associated with different components of the MG are designed using the proposed BGITSMC. Since the design process is the same for each of the MG components, the detailed controller design process is only presented for the BVSC converter with an output LC filter. While, for all other MG components, only the derived control inputs are shown.

### 4.1 BGITSMC design for the BVSC

The BGITSMC approach is employed on a BVSC with an output LC filter to coordinate power-sharing between the AC and DC buses by allowing all state variables linked to the converter to converge to the appropriate steady-state position. Because the suggested approach evaluates the convergences of all connected state variables, the switching control input will be gathered in stages.

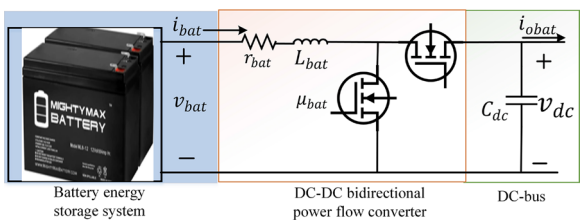


**Fig. 5** The equivalent circuit diagram of the BESS with a DBBC

*Step 1* If the desired value of $V_{dc}$ is $V_{dc(ref)}$, then the tracking error can be written as follows:

$$e_{1VSC} = V_{dc} - V_{dc(ref)} \tag{11}$$

The dynamic of this error is

$$\dot{e}_1 = \frac{i_o}{C_{dc}} - \frac{3}{2V_{dc}C_{dc}}V_{cd}I_{od} + d_1 - \dot{V}_{dc(ref)} \tag{12}$$

To analyze the convergence of $e_1$, the CLF can be written as:

$$W_1 = \frac{1}{2}e_1^2 \tag{13}$$

Using Eq. (12), $\dot{W}_1$ can be written as follows:

$$\dot{W}_1 = e_1\left[\frac{i_o}{C_{dc}} - \frac{3}{2V_{dc}C_{dc}}V_{cd}I_{od} + d_1 - \dot{V}_{dc(ref)}\right] \tag{14}$$

It is critical at this stage to choose a stability function ($\alpha$) that corresponds to the state variable ($V_{cd}$) in Eq. (14) so that $V_{dc} = V_{dc(ref)}$, i.e., $e_{1VSC}$ converges to zero. The following options can be used to do this:

$$\alpha = \frac{2V_{dc}C_{dc}}{3}\left(\frac{i_o}{C_{dc}}\dot{V}_{dc(ref)} - k_1e_1\right) \tag{15}$$

where $k_1$ is a positive design parameter. Using Eq. (15), $\dot{W}_1$ in Eq. (14) can be simplified as follows:

$$\dot{W}_1 = -k_1e_1^2 + e_1d_1 \tag{16}$$

*Step 2* In this step, the error can be defined as follows:

$$e_2 = V_{cd} - \alpha \tag{17}$$

Using Eq. (2), the dynamic of $e_2$ can be written as:

$$\dot{e}_2 = \frac{1}{C_f}I_{id} + \omega V_{cq} - \frac{1}{C_f}I_{od} + d_2 - \dot{\alpha} \tag{18}$$

If $V_{cq(ref)}$ is the reference value of $V_{cq}$, the corresponding tracking error ($e_3$) can be defined as follows:

$$e_3 = V_{cq} - V_{cq(ref)} \tag{19}$$

and its as:

$$\dot{e}_3 = \frac{1}{C_f}I_{iq} - \omega V_{cd} - \frac{1}{C_f}I_{oq} + d_3 - \dot{V}_{cq(ref)} \tag{20}$$

At this time, the second CLF can be selected as follows:

$$W_2 = W_1 + \frac{1}{2}e_2^2 + \frac{1}{2}e_3^2 \tag{21}$$

The derivative of $W_2$ is expressed as follows:

$$\dot{W}_2 = -k_1 e_1^2 + e_1 d_1 + e_2\left[\frac{1}{C_f}I_{id} + \omega V_{cq} - \frac{1}{C_f}I_{od} + d_2 - \dot{\alpha}\right] + e_3\left[\frac{1}{C_f}I_{iq} - \omega V_{cd} - \frac{1}{C_f}I_{oq} + d_3 - \dot{V}_{cq(ref)}\right] \tag{22}$$

Now the stabilizing functions for two-state variables $I_{id}$ and $I_{iq}$ need to be selected and these stabilizing functions are as follows:

$$I_{id} = \alpha_d = -C_f\left(\omega V_{cq} - \frac{1}{C_f}I_{od} - \dot{\alpha} + k_2 e_2\right)$$
$$I_{id} = \alpha_d = -C_f\left[-\omega V_{cd} - \frac{1}{C_f}I_{oq} - \dot{V}_{cq(ref)} + k_3 e_3\right] \tag{23}$$

with $k_2$ and $k_3$ as positive control parameters. Equation (22) can be simplified as:

$$\dot{W}_2 = -k_1 e_1^2 - k_2 e_2^2 - k_3 e_3^2 + e_1 d_1 + e_2 d_2 + e_3 d_3 \tag{24}$$

If $e_1$, $e_2$, and $e_3$ converge to zero, $\dot{W}_2 = 0$ which indicates the negative semi-definiteness of $\dot{W}_2$.

*Step 3* Since $\alpha_d$ and $\alpha_q$ correspond to states $I_{id}$ and $I_{iq}$, these can be defined as in terms of their error variables as defined below:

$$e_4 = I_{id} - \alpha_d$$
$$e_5 = I_{iq} - \alpha_q \tag{25}$$

These errors' dynamics can be expressed as follows:

$$\dot{e}_4 = -\frac{1}{L_f}V_{cd} + \omega I_{iq} + \frac{1}{L_f}V_{dc}M_d + d_4 - \dot{\alpha}_d$$
$$\dot{e}_5 = -\frac{1}{L_f}V_{cq} - \omega I_{id} + \frac{1}{L_f}V_{dc}M_q + d_5 - \dot{\alpha}_q \tag{26}$$

At this point, the global integral terminal sliding surface can be defined as follows:

$$S_d = e_4 + \tau_1 \int e_4 dt + \tau_2 (\int e_4 dt)^{x/y}$$
$$S_q = e_5 + \tau_1 \int e_5 dt + \tau_2 (\int e_5 dt)^{x/y} \tag{27}$$

where $x$ and $y$ are odd values that must meet the condition $1 < \frac{x}{y} < 2$, while $\tau_1$ and $\tau_2$ are positive constants. The dynamic of $S_d$ and $S_q$, using the values of $\dot{e}_{4VSC}$ and $\dot{e}_{5VSC}$, can be written as:

$$\dot{S}_d = -\frac{1}{L_f}V_{cd} + \omega I_{iq} + \frac{1}{L_f}V_{dc}M_d + d_4 - \dot{\alpha}_d + \tau_1 e_4 + \tau_2 \frac{x}{y} e_4 (\int e_4 dt)^{\frac{x}{y}-1}$$
$$\dot{S}_q = -\frac{1}{L_f}V_{cq} - \omega I_{id} + \frac{1}{L_f}V_{dc}M_q + d_5 - \dot{\alpha}_q + \tau_1 e_5 + \tau_2 \frac{x}{y} e_5 (\int e_5 dt)^{\frac{x}{y}-1} \tag{28}$$

The CLF should be chosen as follows to analyze convergences of all errors connected with the BVSC:

$$W_3 = W_2 + \frac{1}{2}S_d^2 + \frac{1}{2}S_q^2 \tag{29}$$

whose derivative can be written as:

$$\dot{W}_3 = -k_1 e_1^2 - k_2 e_2^2 - k_3 e_3^2 + e_1 d_1 + e_2 d_2 + e_3 d_3 + S_d d_4 + S_q d_5 + S_d\left[-\frac{1}{L_f}V_{cd} + \omega I_{iq} + \frac{1}{L_f}V_{dc}M_d - \dot{\alpha}_d + \tau_1 e_4 + \tau_2 \frac{x}{y} e_4 (\int e_4 dt)^{\frac{x}{y}-1}\right] + S_q\left[-\frac{1}{L_f}V_{cq} - \omega I_{id} + \frac{1}{L_f}V_{dc}M_q - \dot{\alpha}_q + \tau_1 e_5 + \tau_2 \frac{x}{y} e_5 (\int e_5 dt)^{\frac{x}{y}-1}\right] \tag{30}$$

For the stability of the entire converter, $\dot{W}_3$ in Eq. (30) needs to be negative semi-definite or negative-definite i.e., $\dot{W}_3 \leq 0$ which will be possible if $M_d$ and $M_q$ are selected as follows:

$$M_d = \frac{L_f}{V_{dc}}\left[\frac{1}{L_f}V_{cd} - \omega I_{iq} + \dot{\alpha}_d - \tau_1 e_4 - \tau_2 \frac{x}{y} e_4 (\int e_4 dt)^{\frac{x}{y}-1} - F_4 sgn(S_d) - k_4 S_d\right] - \frac{e_1}{S_d}F_1 sgn(e_1) - \frac{e_2}{S_d}F_2 sgn(e_2)$$
$$M_q = \frac{L_f}{V_{dc}}\left[\frac{1}{L_f}V_{cq} + \omega I_{id} + \dot{\alpha}_q - \tau_1 e_5 - \tau_2 \frac{x}{y} e_5 (\int e_5 dt)^{\frac{x}{y}-1} - F_5 sgn(S_q) - k_5 S_q\right] - \frac{e_3}{S_q}F_3 sgn(e_3) \tag{31}$$

where $k_4$ and $k_5$ are positive control parameters.

With the switching control inputs in Eq. (31), $\dot{W}_3$ in Eq. (30) can be written as follows:

$$\begin{aligned}\dot{W}_3 = &-k_1e_1^2 - k_2e_2^2 - k_3e_3^2 - k_4e_4^2 - k_5e_5^2 + e_1\big(d_1 - F_1sgn(e_1)\big)\\ &+ e_2\big(d_2 - F_2sgn(e_2)\big) + e_3\big(d_3 - F_3sgn(e_3)\big)\\ &+ S_d\big(d_4 - F_4sgn(S_d)\big) + S_q\big(d_5 - F_5sgn\big(S_q\big)\big)\end{aligned} \tag{32}$$

If the following criteria are met, Eq. (32) will be negative semi-definite:

$|d_1| \le F_1$, $|d_2| \le F_2$, $|d_3| \le F_3$, $|d_4| \le F_4$, and $|d_5| \le F_5$. with $F_1$, $F_2$, $F_3$, $F_4$, and $F_5$ as known bounds. Therefore, the control law as described by Eq. (31) can stabilize the BVSC with an output LC filter. The switching control inputs for the remaining converters can be determined in the same way. However, these design techniques have not been repeated in this paper.

## 5 Proposed controller for the DBC in conjunction with the solar PV unit

The control input for a DBC with a solar PV unit is calculated using the dynamical model provided by Eq. (3). The control input for the DBC in conjunction with the solar PV unit can be obtained using the BGITSMC approach as follows:

$$\begin{aligned}\dot{\mu}_{pv} = -\frac{1}{V_{dc}}\Bigg[&\dot{M}_{pv} + \frac{\mu_{pv}}{C_{dc}}\big[(1-\mu_{pv})i_{Lpv} - i_{opv}\big]\\ &+k_6\dot{e}_6 + k_7e_7 + F_7sgn\big(S_{pv}\big) + \frac{e_6}{S_{pv}}F_6sgn(e_6)\\ &+\tau_3e_7 + \tau_4\frac{x}{y}e_7(\textstyle\int e_7dt)^{\frac{x}{y}-1}\Bigg]\end{aligned} \tag{33}$$

where $e_6$ and $e_7$ are error variables; and $M_1 = \frac{1}{L_{Lpv}}\big[v_{pv} - r_{pv}i_{Lpv} - v_{dc}\big]$ with $k_6$ and $k_7$ as positive control parameters while $F_6$ and $F_7$ are known bounds to EDs with $\big|d_6\big| \le F_6$ and $\big|d_7\big| \le F_7$.

## 6 Proposed controller for the DBC in conjunction with the PMSG farm

In this subsection, he control input will be derived from the dynamical model of the DBC in conjunction with the PMSG-based wind farm, which is represented by Eq. (8). The control law for the PMSG-based wind farm using the BGITSMC approach can be expressed as follows:

$$\dot{u}_R = -\frac{L_r}{V_{dc}}[N + k_9S_{PMSG} + F_9sgn(S_{PMSG}) + \frac{e_8}{S_{PMSG}}F_8sgn(e_8)] \tag{34}$$

where $N = \frac{u_R}{L_rV_{dc}}\big[(1-u_R)i_{L_R} + V_{dc}\big] + \dot{M}_2 + \tau_5e_9 + \tau_6\frac{x}{y}e_9(\int e_9dt)^{\frac{x}{y}-1}$, $M_2 = -\frac{1}{L_r}\big(r_Ri_{L_R} + V_{dc}\big) - \frac{di_{L_{R(ref)}}}{dt} + k_8e_8$,

$e_8$ and $e_9$ are error variables with $k_8$ and $k_9$ as positive control parameters while $F_8$ and $F_9$ are known bounds to EDs with $\big|d_8\big| \le F_8$ and $\big|d_9\big| \le F_9$.

## 7 Proposed controller design for the DBBC in conjunction with the BESS

The switching control input for the DBBC in a BESS is obtained using the dynamical model in Eq. (10). The switching law for the bidirectional DC-DC converter in a BESS can be written using the BGITSMC approach as follows:

$$\begin{aligned}\dot{\mu}_{bat} = \frac{1}{v_{dc}}\Bigg[&\dot{M}_3 - \frac{\mu_{bat}}{C_{dc}}(\mu_{bat}i_{bat} - i_{obat}) + k_{10}\dot{e}_{10}\\ &+k_{11}S_{bat} + F_{11}\mathrm{sgn}(S_{bat})\frac{e_{10}}{S_{bat}}F_{10}sgn(e_{10})\\ &+\tau_7e_9 + \tau_8\frac{x}{y}e_{11}(\textstyle\int e_{11}dt)^{\frac{x}{y}-1}\Bigg]\end{aligned} \tag{35}$$

where $e_{10}$ and $e_{11}$ are error variables; and $M_3 = \frac{1}{L_{bat}}(v_{bat} - r_{bat}i_{bat} - \frac{d}{dt}i_{bat(ref)}$ with $k_{10}$ and $k_{11}$ as positive control parameters while $F_{10}$ and $F_{11}$ are known bounds to EDs with $\big|d_{10}\big| \le F_{10}$ and $\big|d_{11}\big| \le F_{11}$.

## 8 Controller performance evaluation

The dynamic performance of the hybrid AC/DC MG with the proposed controller has been evaluated in this section. A set of simulation studies have been carried out on the MG shown in Fig. 1 using the MATLAB/SIMULINK SimpowerSystem software. Under nominal operating conditions, the DC bus voltage is considered to be 640 V, and the power rating of the solar PV unit is considered to be 12 kW under standard test conditions (1 kW/m$^2$ and 25 °C) in the test MG. It is noted here that in this work, the conventional Perturb & Observe (P & O) method is used as a Maximum Power Point Tracking (MPPT) algorithm to extract the maximum power from the solar PV unit. The PMSG-based wind farm is rated at 25 kW. A Lithium-ion battery with a capacity of 150 Ah and a nominal voltage of 300 V has been considered for the MG. The maximum load demand on the DC side of the MG is considered to be 25 kW, while the maximum load on the AC side is considered to be 30 kW. The generalized implementation block structure of the proposed control scheme is presented in Fig. 6. The developed controller, as seen in this diagram, employs physical attributes like voltage, current, and so on as feedback from the system, while the system model incorporates EDs such as

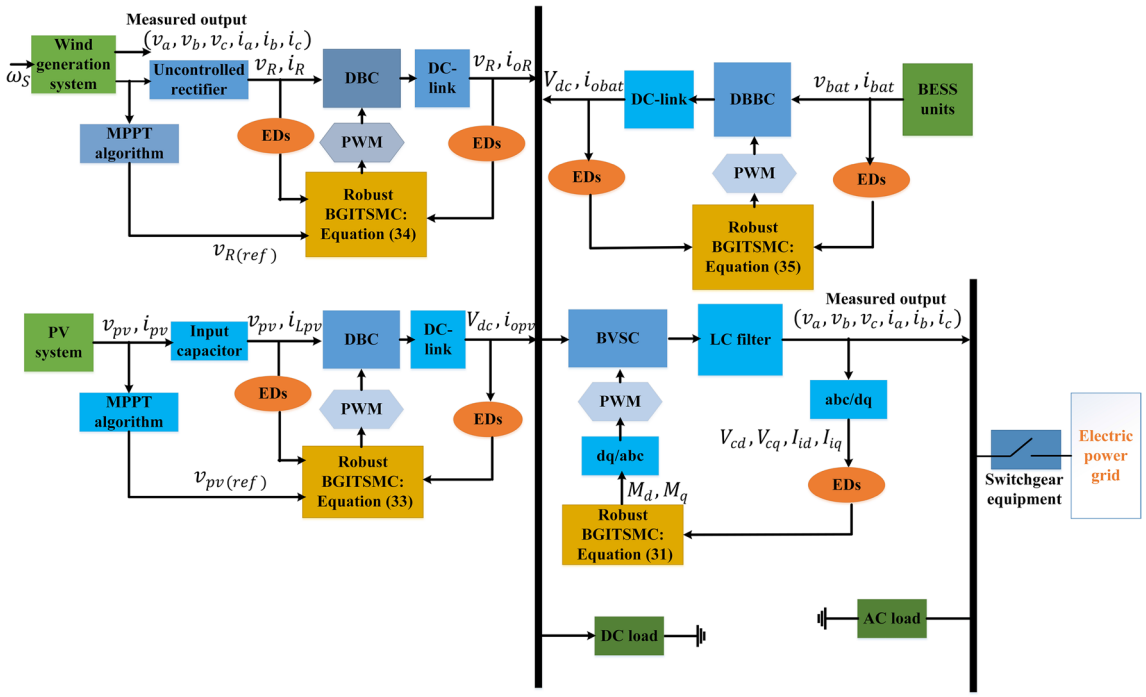


**Fig. 6** Implementation block diagram of the proposed control scheme

parameter fluctuations, measurement noises, and modeling errors. The impacts of measurement noises are captured in the form of white Gaussian noises, and the bounds on EDs for individual components are derived based on deviations in parameters from their nominal values, combined with modeling errors. These physical attributes, combined with the ED boundaries and nominal parameters of the individual components, are utilized to create the control signal, which is then employed to assure the system's dynamic performance. The control signals for all components of the MG are derived from MATLAB/SIMULINK SimPowerSystems, as illustrated in Fig. 1. The switching frequencies of the converters during the simulation study are set to 5 kHz, while the sampling frequency of the simulation study is considered to be 10 kHz. The system parameters of the proposed hybrid MG system and the gain parameters of the designed controller are mentioned in Tables 1 and 2, respectively.

The DC part of the hybrid AC/DC MG is assumed to run initially in this scenario, with the DC-bus voltage being produced by the first activation of the solar PV unit. The PMSG-based wind farm is then put into service, followed by the BESS and the DC load. Once the DC component is completely operational, AC loads are turned on. By evaluating a variety of operating scenarios, the performance of the developed BGITSMC is compared to that of a typical SMC as reported in [39]. It should be mentioned that the existing SMC is designed by considering an integral sliding surface along with the inclusion of a conventional reaching law.

During the simulation study, from time t = 0 to 2 s, the irradiation is considered to be 880 W/m$^2$, which causes a solar PV power output of 9.52 kW. The PMSG-based wind farm is considered to produce 13.7 kW of power during this time period, while operating under a wind speed of 9 m/s. The load demand during this period is considered to be 5.85 kW DC load and 10.44 kW AC load, respectively. During the time period t = 0–2 s, the overall power generation on the DC-side is 23.22 kW, while the DC load demand is 5.85 kW. This indicates that there will be a surplus generation of 17.37 kW of DC power. Depending on the SOC of the battery and the loads in the system, the additional power from the DC side can be either stored or transferred to the AC side. Since the AC load requirement during the time period t = 0–2 s is 10.44 kW, this load demand is met by importing power from the DC side by modulating the bidirectional VSC's switching control signal. The battery stores the energy equivalent to the remaining residual power on the DC-side because it still has the potential to store energy. However, the battery charging power is 4.098 kW, i.e., the power loss is 2.8 kW. Figure 7 shows the breakdown of the power in different components of the MG during this time period. The DC-link voltage is shown in Fig. 8, which is maintained at its desired value. As can be seen

**Table 1** Nominal parameters of the proposed hybrid AC/DC MG

| Parameters | Values |
|---|---|
| *BVSC* | |
| Capacitor of a LC filter, C*f* | 6.85 μF |
| Inductor of a LC filter, L*f* | 2 mH |
| AC load | 0∼30 kW |
| *Solar PV unit* | |
| Maximum output power of a PV system, P*pv* | 12 kW |
| PV voltage at MPPT, V*mp* | 31 V |
| PV current at MPPT, i*mp* | 8.06 A |
| Resistance of the DBC, r*Lpv* | 0.05 Ω |
| Inductance of the DBC, L*Lpv* | 0.352 mH |
| Input capacitance of the solar PV unit | 2200 μF |
| *BESS (Lithium-ion battery)* | |
| Nominal voltage of a BESS, v*bat* | 300 V |
| Rated capacity of a BESS, Q*bat* | 150 Ah |
| Resistance of the BDDC converter, r*bat* | 0.08 Ω |
| Inductance of the BDDC converter, L*bat* | 1 mH |
| *PMSG unit* | |
| Output power of a wind generator, P*wind* | 25 kW |
| Stator resistance of a wind generator, R*s* | 0.425 Ω |
| Stator inductance of a wind generator, L*s* | 1.67 mH |
| Stator flux of a wind generator, ψ | 0.433 |
| Resistance of the DBC, r*R* | 0.04 Ω |
| Inductance of the DBC, L*R* | 0.2 mH |
| *Common DC-bus* | |
| Rated voltage of the common DC-bus, V*(dc-ref)* | 640 V |
| Capacitance of the common DC-bus, C*dc* | 1200 μF |
| Range of the DC load power, P*DC-Load* | 0∼25 kW |

**Table 2** Control parameters of the proposed control scheme

| Parameters | Values |
|---|---|
| *Control parameters for a BVSC* | |
| *k*1, *k*2, *k*3, *k*4 | 150, 180, 200, 170 |
| *k*5, *τ*1, *τ*2, *F*1, *F*2 | 250, 30, 40, 0.8, 0.8 |
| *F*3, *F*4, *F*5, *x*, *y* | 0.8, 0.8, 0.8, 13, 7 |
| *Control parameters for a solar PV unit* | |
| *k*6, *k*7, *τ*3 | 220, 250, 25 |
| *τ*4, *F*6, *F*7 | 35, 0.8, 0.8 |
| *Control parameters for a PMSG unit* | |
| *k*8, *k*9, *τ*5 | 180, 250, 15 |
| *τ*6, *F*8, *F*9 | 18, 0.8, 0.8 |
| *Control parameters for a BESS unit* | |
| *k*10, *k*11, *τ*7 | 260, 290, 40 |
| *τ*8, *F*10, *F*11 | 50, 0.8, 0.8 |

from Figs. 7 and 8, the performance of the proposed BGITSMC and the ESMC are the same during this time period, as there is no transient event during this period.

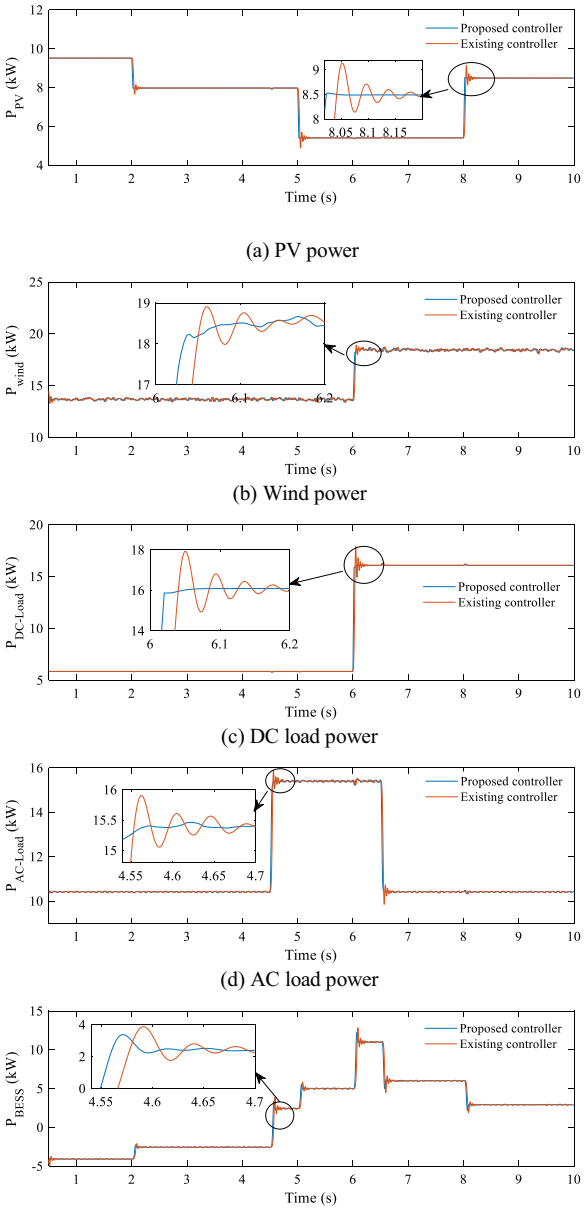


**Fig. 7** Under different operating conditions, the power profile of the **a** solar PV unit, **b** wind generator, **c** DC load, **d** AC load, and **e** BESS

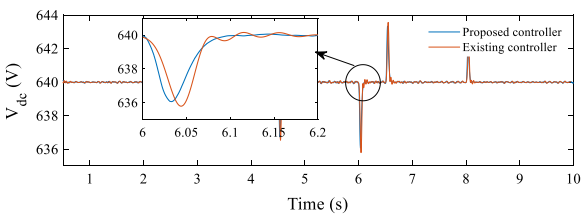


**Fig. 8** Under changing operational circumstances, the DC-bus voltage

In order to demonstrate the performance of the proposed controller at t = 2 s, the following change in condition is considered:

- The power generation from the solar PV unit decreases from 9.52 to 7.98 kW as shown in Fig. 7a.

All other conditions, however, remain the same as in the time period t = 0–2 s until t = 4.5 s. During this time period, the DC-side continues to generate more power than the load demand, while the AC-side continues to have a shortfall in power generation. The generated from the DC side, on the other hand, is exported to the AC side to maintain power balance. The battery will now retain less power since the overall power surplus is lower than in the previous stage, as seen in Fig. 7e. Transients disrupt the power profiles of different components and the DC-link voltage in a hybrid AC/DC microgrid at t = 2 s, as illustrated in Figs. 7 and 8, and the designed BGITSMC handles these transients better (in terms of overshoot and settling time) than the ESMC. As shown in Fig. 7d, the AC load changes from 10.44 to 15.4 kW at t = 4.5 s. All remaining components' power profiles are comparable to those of the prior operating state, i.e., from t = 4.5 s to t = 5 s.

The hybrid AC/DC microgrid experiences another transient event from t = 5–6 s due to the following changes:

- As shown in Fig. 7a, the sun irradiation decreases from 700 to 500 W/m$^2$, causing the output power of the solar PV unit to decrease from 7.98 to 5.42 kW.

All other conditions remain unchanged. During this time period, the bidirectional VSC will export the same amount of power from the DC side to the AC side as previously explained. However, as total generation is less than total load demand, the energy released by the battery is used to maintain power balance, as illustrated by the BESS power profile in Fig. 7e.

The power profiles of the hybrid AC/DC microgrid are disturbed at t = 6 s due to the following event:

- As illustrated in Fig. 7b, the wind speed increases from 9 to 13 m/s, raising the output power of the PMSG-based wind farm from 13.7 to 18.5 kW and
- As seen in Fig. 7c, the DC load increases from 5.85 to 16.09 kW.

Other operating conditions remain unchanged as those of the previous time period (i.e., from t = 5 s to t = 6 s) and until t = 6.5 s. The overall generation on the DC side is 23.9 kW during this time period, whereas the load demand is 16.09 kW. At the same time, the AC-side load requirement is 15.4 kW. At this moment, to maintain the power balance, the battery discharges its power as shown in Fig. 7e. In comparison to all other scenarios, the DC-link voltage is drastically disrupted during these transients. However, as compared to the ESMC, the proposed BGITSMC can effectively stabilize this. The AC load is reduced from 15.40 to 10.44 kW at t = 6.5 s while all reaming components run with power profiles comparable to the preceding phase, and this operation is monitored until t = 8 s.

Finally, at t = 8 s, the solar PV unit power changes from 5.41 to 8.5 kW, while all reaming components operate with comparable power profiles to the previous period, and this operating condition remains unchanged until t = 10 s. The bidirectional VSC transfers 10.44 kW of power from the DC-side to the AC-side in this scenario, and the BESS releases less energy than in the previous time period. Because the intensity of this transient is minor, it has little effect on the power profiles of different components, as seen in Fig. 7. However, as seen in Fig. 8, the DC-link voltage is marginally influenced, but the effect is significantly less severe than under normal conditions. Tables 3, 4, 5, 6, 7 and 8 display the overshoot/undershoot and settling time for the solar PV unit power, PMSG power, DC load power, AC load power, BESS

**Table 3** Quantitative analysis for a solar PV unit

| Transient time (s) | Settling time (ms) | | Overshoot/undershoot (%) | |
|---|---|---|---|---|
| | Proposed | Existing | Proposed | Existing |
| 2 | 0 | 100 | 0 | 2.50 |
| 5 | 0 | 150 | 0 | 5 |
| 8 | 0 | 210 | 0 | 5.88 |

**Table 4** Quantitative analysis for a wind power system

| Transient time (s) | Settling time (ms) | | Overshoot/undershoot (%) | |
|---|---|---|---|---|
| | Proposed | Existing | Proposed | Existing |
| 6 | 50 | 210 | 0 | 2.70 |

**Table 5** Quantitative analysis for DC load power

| Transient time (s) | Settling time (ms) | | Overshoot/undershoot (%) | |
|---|---|---|---|---|
| | Proposed | Existing | Proposed | Existing |
| 6 | 25 | 200 | 0 | 12.50 |

**Table 6** Quantitative analysis for AC load power

| Transient time (s) | Settling time (ms) | | Overshoot/undershoot (%) | |
|---|---|---|---|---|
| | Proposed | Existing | Proposed | Existing |
| 4.5 | 50 | 200 | 0 | 3.50 |
| 6.5 | 40 | 190 | 0 | 3.70 |

**Table 7** Quantitative analysis for BESS power

| Transient time (s) | Settling time (ms) | | Overshoot/undershoot (%) | |
|---|---|---|---|---|
| | Existing | Proposed | Proposed | Existing |
| 2 | 31 | 60 | 11.88 | 20.78 |
| 4.5 | 99 | 210 | 40 | 70 |
| 5 | 50 | 130 | 25 | 40.25 |
| 6 | 100 | 250 | 44.22 | 80.50 |
| 6.5 | 90 | 210 | 42.30 | 75.15 |
| 8 | 80 | 170 | 29.12 | 52.62 |

**Table 8** Quantitative analysis for DC-bus voltage

| Transient time (s) | Settling time (ms) | | Overshoot/undershoot (%) | |
|---|---|---|---|---|
| | Existing | Proposed | Proposed | Existing |
| 2 | 35 | 70 | 0.10 | 0.156 |
| 4.5 | 100 | 200 | 0.32 | 0.468 |
| 5 | 42 | 120 | 0.26 | 0.3125 |
| 6 | 100 | 205 | 0.42 | 0.625 |
| 6.5 | 90 | 170 | 0.35 | 0.468 |
| 8 | 50 | 130 | 0.27 | 0.3125 |

power, and DC-bus voltage, respectively under various transient scenarios for both controllers. The designed controller outperforms the existing controller in terms of overshoot and settling time, as shown by the quantitative findings shown in Tables 3, 4, 5, 6, 7 and 8.

The efficacy of the developed BGISMC to maintain the dynamic stability of the hybrid AC/DC MG by balancing power is clearly demonstrated by simulation results under various transient events. This demonstrates the resiliency of the proposed controller against any variation in MG operating conditions.

## 9 Conclusion

A robust backstepping global integral terminal sliding mode control approach to ensure the dynamic stability of hybrid AC/DC MGs under varying operating conditions has been presented in this paper. The control system derives control inputs for different components of the hybrid MG, while ensuring convergence of all the MG states to their desired values. The rate of change of energy associated with distinct states is observed, and the dynamic stability is theoretically studied using control Lyapunov functions. External disturbances are characterized in terms of parametric uncertainties, modeling errors, and external disturbances that are constrained in such a manner that the proposed controllers maintain dynamic stability in every situation. To support the theoretical conclusions, simulation tests were undertaken, and it was discovered that the developed controllers increase the dynamic stability of hybrid AC/DC MGs by reducing overshoots and settling periods compared to existing approaches. However, certain problems arise during the implementation of the planned controller, which are mostly related to the controller's gain parameter selection. To avoid these difficulties, artificial intelligence can be integrated with the control strategy created.

#### Abbreviations

| | |
|---|---|
| BGITSMC | Backstepping global integral terminal sliding mode controller |
| PV | Solar photovoltaic |
| BESS | Battery energy storage system |
| CLF | Control Lyapunov function |
| SMC | Sliding mode control |
| GHG | Greenhouse gas |
| RES | Renewable energy source |
| DG | Distributed generation |
| ESS | Energy storage system |
| MG | Microgrid |
| PI | Proportional-integral |
| MPBPC | Multiple parallel bidirectional power converter |
| ANN | Adaptive neural network |
| EDs | External disturbances |
| BVSC | Bidirectional voltage source converter |
| DBC | DC-DC boost converter |
| DBBC | DC-DC bidirectional converter |
| P & O | Perturb & observe |
| MPPT | Maximum power point tracking |

#### Acknowledgements

Not applicable.

#### Author contributions

Conceptualization, TKR and SKG; methodology, TKR and SS; software, TKR and SKG; validation, TKR and SKG; formal analysis, TKR; investigation, TKR; writing—original draft preparation, TKR and SKG; writing—review and editing, TKR, SKG and SS; supervision, TKR and SS; and project administration, TKR and SS. All authors read and approved the final version of the manuscript.

#### Funding

Not applicable.

#### Availability of data and materials

Not applicable.

### Declarations

#### Competing interests

The authors declare that they have no known competing financial interests or personal relationships that could have appeared to influence the work reported in this paper.

Received: 19 April 2022 Accepted: 15 February 2023
Published online: 28 February 2023

**References**


1. Roy, T. K., & Mahmud, M. A. (2017). Active power control of three-phase grid-connected solar PV systems using a robust nonlinear adaptive backstepping approach. *Solar Energy, 153*, 64–76.
2. Singh, B., Pathak, G., & Panigrahi, B. K. (2017). Seamless transfer of renewable-based microgrid between utility grid and diesel generator. *IEEE Transactions on Power Electronics, 33*(10), 8427–8437.
3. Magdy, G., Mohamed, E. A., Shabib, G., Elbaset, A. A., & Mitani, Y. (2018). Microgrid dynamic security considering high penetration of renewable energy. *Protection and Control of Modern Power Systems, 3*(1), 1–11.
4. Roy, T. K., Mahmud, M. A., Oo, A. M. T., Haque, M. E., Muttaqi, K. M., Mendis, N. (2016) Nonlinear adaptive backstepping controller design for controlling bidirectional power flow of BESSs in DC microgrids. In *2016 IEEE industry applications society annual meeting*. IEEE pp. 1–8
5. Papari, B., Edrington, C. S., Bhattacharya, I., & Radman, G. (2017). Effective energy management of hybrid AC–DC microgrids with storage devices. *IEEE Transactions on Smart Grid., 10*(1), 193–203.
6. Ding, G., Gao, F., Zhang, S., Loh, P. C., & Blaabjerg, F. (2014). Control of hybrid AC/DC microgrid under islanding operational conditions. *Journal of Modern Power Systems and Clean Energy., 2*(3), 223–232.
7. Firuzi, M. F., Roosta, A., & Gitizadeh, M. (2019). Stability analysis and decentralized control of inverter-based ac microgrid. *Protection and Control of Modern Power Systems., 4*(1), 1–24.
8. Roy, T. K., Mahmud, M. A., Oo, A. M. T., Haque, M. E., Muttaqi, K. M., & Mendis, N. (2018). Nonlinear adaptive backstepping controller design for islanded DC microgrids. *IEEE Transactions on Industry Applications., 54*(3), 2857–2873.
9. Liu, S., Zhou, C., Guo, H., Shi, Q., Song, T. E., Schomer, I., et al. (2021). Operational optimization of a building-level integrated energy system considering additional potential benefits of energy storage. *Protection and Control of Modern Power Systems., 6*(1), 1–10.
10. Ghosh, S. K., Roy, T. K., Pramanik, M. A. H., Sarkar, A. K., Mahmud, M., et al. (2020). An energy management system-based control strategy for DC microgrids with dual energy storage systems. *Energies, 13*(11), 2992.
11. Mahmud, M. A., Roy, T. K., Saha, S., Haque, M. E., & Pota, H. R. (2019). Robust nonlinear adaptive feedback linearizing decentralized controller design for islanded DC microgrids. *IEEE Transactions on Industry Applications., 55*(5), 5343–5352.
12. Chen, D., & Xu, L. (2012). Autonomous DC voltage control of a DC microgrid with multiple slack terminals. *IEEE Transactions on Power Systems., 27*(4), 1897–1905.
13. Loh, P. C., Li, D., Chai, Y. K., & Blaabjerg, F. (2012). Hybrid AC–DC microgrids with energy storages and progressive energy flow tuning. *IEEE Transactions on Power Electronics., 28*(4), 1533–1543.
14. Alnejaili, T., Drid, S., Mehdi, D., Chrifi-Alaoui, L., Belarbi, R., & Hamdouni, A. (2015). Dynamic control and advanced load management of a stand-alone hybrid renewable power system for remote housing. *Energy Conversion and Management., 105*, 377–392.
15. Simpson-Porco, J. W., D¨orfler, F., & Bullo, F. (2016). Voltage stabilization in microgrids via quadratic droop control. *IEEE Transactions on Automatic Control., 62*(3), 1239–1253.
16. Gupta, A., Doolla, S., & Chatterjee, K. (2017). Hybrid AC–DC microgrid: Systematic evaluation of control strategies. *IEEE Transactions on Smart Grid., 9*(4), 3830–3843.
17. Sun, Q., Zhou, J., Guerrero, J. M., & Zhang, H. (2014). Hybrid three-phase/single-phase microgrid architecture with power management capabilities. *IEEE Transactions on Power Electronics., 30*(10), 5964–5977.
18. Nejabatkhah, F., & Li, Y. W. (2014). Overview of power management strategies of hybrid AC/DC microgrid. *IEEE Transactions on Power Electronics., 30*(12), 7072–7089.
19. Li, P., & Zheng, M. (2019). Multi-objective optimal operation of hybrid AC/DC microgrid considering source-network-load coordination. *Journal of Modern Power Systems and Clean Energy., 7*(5), 1229–1240.
20. Chinchilla, M., Arnaltes, S., & Burgos, J. C. (2006). Control of permanent-magnet generators applied to variable-speed wind-energy systems connected to the grid. *IEEE Transactions on Energy Conversion., 21*(1), 130–135.
21. Ackermann, T. (2005). *Wind power in power systems* (Vol. 200). Wiley.
22. Nguyen, H. T., Kim, E. K., Kim, I. P., Choi, H. H., & Jung, J. W. (2017). Model predictive control with modulated optimal vector for a three-phase inverter with an LC filter. *IEEE Transactions on Power Electronics., 33*(3), 2690–2703.
23. Liu, X., Wang, P., & Loh, P. C. (2011). A hybrid AC/DC microgrid and its coordination control. *IEEE Transactions on Smart Grid., 2*(2), 278–286.
24. Ma, T., Cintuglu, M. H., & Mohammed, O. A. (2016). Control of a hybrid AC/DC microgrid involving energy storage and pulsed loads. *IEEE Transactions on Industry Applications., 53*(1), 567–575.
25. Sowmmiya, U., & Govindarajan, U. (2017). Control and power transfer operation of WRIG-based WECS in a hybrid AC/DC microgrid. *IET Renewable Power Generation., 12*(3), 359–373.
26. Xia, Y., Peng, Y., Yang, P., Yu, M., & Wei, W. (2016). Distributed coordination control for multiple bidirectional power converters in a hybrid AC/DC microgrid. *IEEE Transactions on Power Electronics., 32*(6), 4949–4959.
27. Loh, P. C., Li, D., Chai, Y. K., & Blaabjerg, F. (2012). Autonomous operation of hybrid microgrid with AC and DC subgrids. *IEEE Transactions on Power Electronics., 28*(5), 2214–2223.
28. Wang, J., Jin, C., & Wang, P. (2017). A uniform control strategy for the interlinking converter in hierarchical controlled hybrid AC/DC microgrids. *IEEE Transactions on Industrial Electronics., 65*(8), 6188–6197.
29. Armghan, H., Yang, M., Wang, M., Ali, N., & Armghan, A. (2020). Nonlinear integral backstepping based control of a DC microgrid with renewable generation and energy storage systems. *International Journal of Electrical Power & Energy Systems., 117*, 105613.
30. Li, P., Guo, T., Zhou, F., Yang, J., & Liu, Y. (2020). Nonlinear coordinated control of parallel bidirectional power converters in an AC/DC hybrid microgrid. *International Journal of Electrical Power & Energy Systems., 122*, 106208.
31. Armghan, H., Yang, M., Armghan, A., Ali, N., Wang, M., & Ahmad, I. (2020). Design of integral terminal sliding mode controller for the hybrid AC/DC microgrids involving renewables and energy storage systems. *International Journal of Electrical Power & Energy Systems., 119*, 105857.
32. Akpolat, A. N., Habibi, M. R., Baghaee, H. R., Dursun, E., Kuzucuoglu, A. E. E., Yang, Y. (2021) Dynamic stabilization of DC microgrids using ANN-based model predictive control. *IEEE Transactions on Energy Conversion*.
33. Chettibi, N., Mellit, A., Sulligoi, G., & Pavan, A. M. (2016). Adaptive neural network-based control of a hybrid AC/DC microgrid. *IEEE Transactions on Smart Grid., 9*(3), 1667–1679.
34. Kang, K. M., Choi, B. Y., Lee, H., An, C. G., Kim, T. G., Lee, Y. S., et al. (2021). Energy management method of hybrid AC/DC microgrid using artificial neural network. *Electronics, 10*(16), 1939.
35. Roy, T. K., & Mahmud, M. A. (2017). Dynamic stability analysis of hybrid islanded DC microgrids using a nonlinear backstepping approach. *IEEE Systems Journal., 12*(4), 3120–3130.
36. Wang, C., Li, X., Guo, L., & Li, Y. W. (2014). A nonlinear-disturbance-observer-based DC-bus voltage control for a hybrid AC/DC microgrid. *IEEE Transactions on Power Electronics., 29*(11), 6162–6177.
37. Roy, T. K., Mahmud, M. A. (2021). Fault current compensations in resonant grounded distribution systems to mitigate powerline bushfires using a nonsingular terminal sliding model controller. *IET Generation, Transmission & Distribution*.
38. Roy, T., Mahmud, M. A., Ghosh, S., Pramanik, M., Kumar, R., Oo, A. M. (2021) Design of an adaptive sliding mode controller for rapid earth fault current limiters in resonant grounded distribution networks to mitigate powerline bushfires. In *2021 IEEE Texas Power and Energy Conference (TPEC)*. IEEE. p. 1–6
39. Alam, F., Ashfaq, M., Zaidi, S. S., Memon, A. Y. (2016) Robust droop control design for a hybrid AC/DC microgrid. In *2016 UKACC 11th international conference on control (CONTROL)*. IEEE. pp. 1–6.
40. Baghaee, H. R., Mirsalim, M., Gharehpetian, G. B., Talebi, H. A. (2017) A decentralized power management and sliding mode control strategy for hybrid AC/DC microgrids including renewable energy resources. *IEEE Transactions on Industrial Informatics*.
41. Hassan, M., Paracha, Z. J., Armghan, H., Ali, N., Said, H. A., Farooq, U., et al. (2020). Lyapunov based adaptive controller for power converters used in hybrid energy storage systems. *Sustainable Energy Technologies and Assessments., 42*, 100853.